Geoscience Frontiers 7 (2016) 211–220

HOSTED BY

ELSEVIER

Contents lists available at ScienceDirect

China University of Geosciences (Beijing)

Geoscience Frontiers

journal homepage: www.elsevier.com/locate/gsf

Research paper

Late Palaeogene emplacement and late Neogene–Quaternary exhumation of the Kuril island-arc root (Kunashir island) constrained by multi-method thermochronometry

J. De Grave [a,*], F.I. Zhimulev [b], S. Glorie [c], G.V. Kuznetsov [b], N. Evans [d], F. Vanhaecke [e], B. McInnes [d]

[a] Department of Geology and Soil Science, Mineralogy and Petrology Research Unit, Ghent University, Ghent, Belgium
[b] Institute of Geology and Mineralogy, Siberian Branch, Russian Academy of Sciences, Novosibirsk, Russia
[c] Tectonics, Resources and Exploration (TraX), Department of Earth Sciences, School of Physical Sciences, University of Adelaide, Adelaide, Australia
[d] John De Laeter Center for Isotope Research, Applied Geology/Applied Physics, Curtin University, Perth, Australia
[e] Department of Analytical Chemistry, Atomic and Mass Spectrometry Research Unit, Ghent University, Ghent, Belgium

ARTICLE INFO

Article history:
Received 2 February 2015
Received in revised form
4 May 2015
Accepted 18 May 2015
Available online 9 June 2015

Keywords:
Kuril island arc
Kunashir island
Northwest pacific
Thermochronometry
Zircon U-Pb dating

ABSTRACT

The Kuril islands constitute a volcanic island arc-trench system, stretching from eastern Hokkaido (Japan) to Kamchatka (Russia) along the northwestern Pacific subduction system. The current arc consists of several volcanic islands mainly with Neogene basement and capped by several, predominantly andesitic, active subduction stratovolcanoes. Kunashir Island is the southwestern-most island of the arc, just off the Hokkaido coast and represents the study area in this paper. The island is composed of a Lower Complex of mainly late Miocene to Pliocene volcanic rocks, covered by an Upper Complex of younger (basaltic) andesitic lava flows and tuffs on which currently four active volcanic edifices are built. In the Lower Complex sub-volcanic and deeper-seated intrusives of the so-called Prasolov and Dokuchaev magmatic complexes are found. More differentiated, tonalitic–granodioritic rocks were collected from these small intrusive bodies. An early Oligocene zircon LA-ICP-MS U/Pb age of 31 Ma for the Prasolov Complex was obtained, showing that the basement of Kunashir Island is older than previously thought. Thermochronometry (apatite fission-track and U-Th-Sm/He and zircon U-Th/He analyses) further shows that the magmatic basement of the island was rapidly exhumed in the Pleistocene to present levels in a differential pattern, with He-ages ranging from 1.9 to 0.8 Ma. It is shown that the northern section of the island was hereby exhumed more intensely.

1. Introduction and tectonic setting

The Kuril Islands represent a volcanic island arc in the Northwest Pacific Ocean, outlining the convergent plate boundary between the Pacific and Okhotsk plates (Fig. 1). Along the Kuril–Kamtchatka trench the Pacific Plate subducts (north)westwards at an average rate of 78–79 mm/yr (Seno et al., 1996). The Okhotsk Plate is thought to be a distinct lithospheric plate in between the North American, Eurasian, Pacific, and Amurian plates (Cook et al., 1986; Seno et al., 1996; Apel et al., 2006) and is largely covered by the current Okhotsk Sea (Fig. 1). Collision of the Okhotsk block with the eastern Siberian margin of Eurasia is thought to have occurred in the late Cretaceous–early Paleocene (~65–55 Ma; e.g., Worrall et al., 1996; Schellart et al., 2003). The geochemistry and petrogenesis of the Kuril Island volcanic rocks have been described by Bailey et al. (1987, 1989), Zhuravlev et al. (1987), Avdeiko et al. (1991), Bailey (1996), Bindeman and Bailey (1999) and Martynov et al. (2010a).

The Kuril arc and trench links the Russian Kamchatka peninsula with Hokkaido, Japan and connects the Aleutian with the Japanese arc-trench (Fig. 1). The Kuril island arc (or Great Kuril Chain), is composed of a sequence of volcanic islands (active subduction

* Corresponding author. Department of Geology and Soil Science (WE13), MINPET, Ghent University, Krijgslaan 281/S8, WE13, B-9000 Gent, Belgium. Tel.: +32 9264 4564.
E-mail address: Johan.DeGrave@UGent.be (J. De Grave).
Peer-review under responsibility of China University of Geosciences (Beijing).

http://dx.doi.org/10.1016/j.gsf.2015.05.002

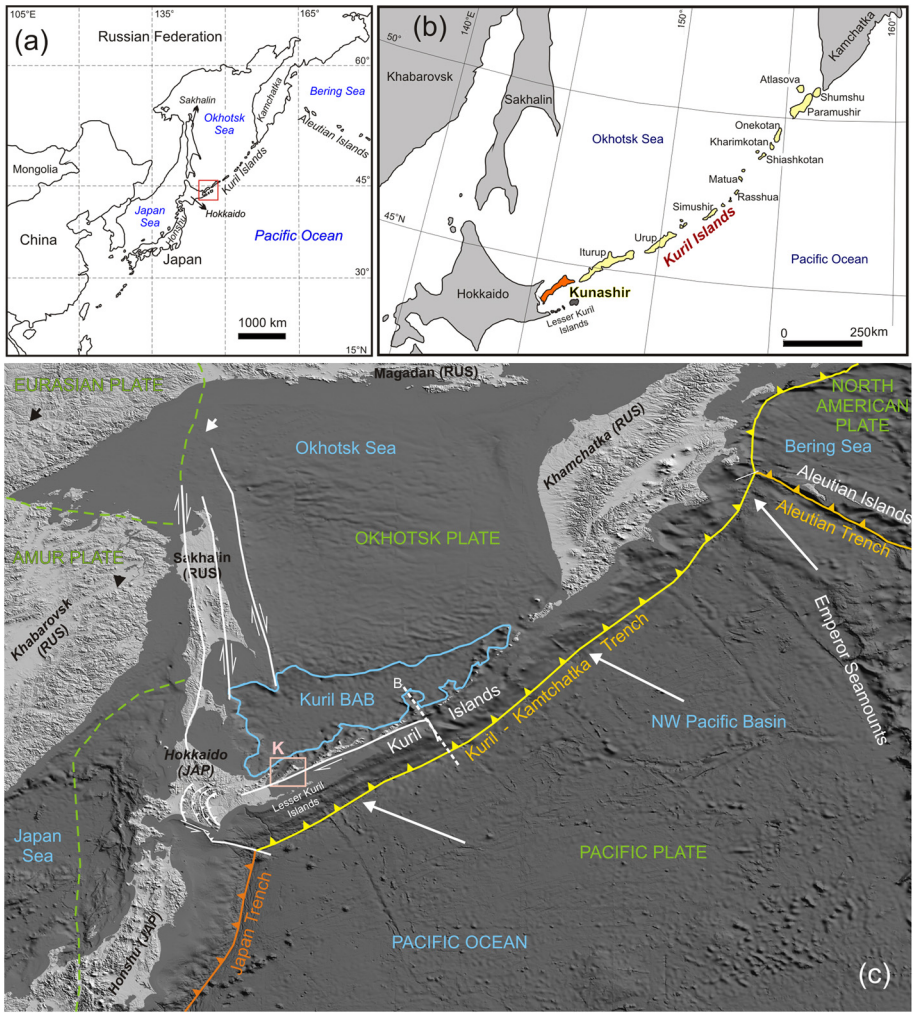

Figure 1. (a) General location of the Kuril Island arc in the Northwest Pacific, (b) position of Kunashir Island in the Kuril arc and general regional geographic setting, and (c) tectonic sketch map of the Kuril island arc. The study area, the island of Kunashir (K), is indicated by the red box.

strato-volcanoes) of 1150 km with average basal width of ~100–200 km (Martynov et al., 2010b). The westernmost Island, Kunashir, represents our study area. To the NE, larger (e.g., Iturup, Urup, Simushir, Onekotan, Paramushir, Shumshu) and smaller (e.g., Rasshua, Matua, Shiashkotan, Kharimkotan) islands delineate the arc (Fig. 1). It is thought that the current volcanic arc developed from late Oligocene to early Miocene.

A second arc, the Lesser Kuril Islands (or Nemuro-Shikotan arc), is located on the Pacific side, south of Kunashir, and includes the Nemuro Peninsula of Hokkaido (Fig. 1). It is envisaged that this paleo-arc constitutes the basement of the modern Kuril arc (Maeda, 1990). While eastern Hokkaido is part of the Kuril arc, central and western Hokkaido are part of the Japan arc (e.g., Wakita, 2013). Oblique subduction of the Pacific Plate along the Kuril trench and associated relative southwestward movement of the Kuril fore-arc eventually led to the Kuril-Japan arc-arc collision in the Miocene (~12 Ma) (Maeda, 1990; Bazhenov and Burtman, 1994; Kusunoki and Kimura, 1998). This collision is ongoing and results in compressive forces in the region and is responsible for the development of the Hidaka Mountains (central Hokkaido) (Fig. 1c; Kimura, 1981, 1986; Kusunoki and Kimura, 1998). The late Miocene arc–arc collision effectively resulted in the exhumation of the lower crustal rocks of the Kuril arc in eastern Hokkaido (Kusunoki and Kimura, 1998).

The Kuril Basin is a prominent wedge-shaped back-arc basin (Fig. 1) where sea-floor spreading occurred in the late Miocene (Savostin et al., 1983; Maeda, 1990; Fournier et al., 1994; Jolivet et al., 1994; Worrall et al., 1996; Baranov et al., 2002; Schellart et al., 2003). The Sakhalin–Hokkaido extensional system still constitutes an active dextral shear system, defining the boundary between the Okhotsk and the Eurasian (Amurian) plate (Fig. 1). Kinematics changed dramatically during the late Miocene from transtension to transpression (Worrall et al., 1996). The latter authors link these movements to far-field effects of the India-Eurasia collision (e.g., Molnar and Tapponnier, 1975; De Grave et al., 2007). The Okhotsk Sea now covers most of the thinned continental crust of the Okhotsk plate, along with the oceanic crust of the deeper (~3300 m) Kuril back-arc basin. The extension and thinning in the Okhotsk plate mainly occurred during the Eocene until the early Miocene (Worrall et al., 1996), while opening of the Kuril Basin is a posterior event, lasting until the late Miocene (early Pliocene?) (e.g., Maeda, 1990; Schellart et al., 2003). High heat flux and the presence of Pleistocene (0.84–1.07 Ma) submarine volcanic rocks suggest that the Kuril back-arc basin might still be active or was active far later than previous thought (Tararin et al., 2000; Baranov et al., 2002; Martynov et al., 2010a).

Late Cretaceous–Paleocene clastic sediments shed off the southern margin of the Okhotsk block were included in the

basement of the Paleo-Kuril (or Lesser Kuril or Nemuro-Shikotan) arc, before it was rifted from Okhotsk by Miocene extension in the Kuril back-arc basin.

Kunashir, the southernmost island of the Kuril arc extends for 123 km (NE–SW), with 7–30 km wide and covers an area of 1,490 km^2. The island is an amalgamate of several volcanic edifices, of which four are active: Tyatya (1,819 m), Ruruy (1,485 m), Mendeleev (886 m) and Golovnin (541 m) (Fig. 2). The current relief of Kunashir is rugged and mountainous and geomorphologically very young, with steep slopes and numerous waterfalls. In the sense of relief, the island is clearly asymmetric: the western or Okhotsk shore is very steep and high, while the eastern or Pacific side is more flat and shallow.

In comparison to the Japan arc, evolution of the main Kuril arc system in an absolute time frame has been studied to a far lesser extent, especially with respect to modern geochronological techniques. This paper provides first zircon U/Pb ages on the volcanic basement and thermochronological ages for the rocks of Kunashir Island with the aim at providing an absolute time frame for their emplacement and subsequent exhumation.

2. Geological setting of Kunashir island

2.1. General setting

The volcanic rocks of the Kuril Islands in general can be divided into two structural levels: (1) a lower level, typically composed of moderately deformed Neogene rocks, and (2) an upper level containing Pleistocene to recent volcanics. In composition these rocks range from basalt to rhyolite, with a predominance of (basaltic) andesites (e.g., Martynov et al., 2010b).

The geology of Kunashir Island can also be described in this perspective, with two structural levels (Fig. 2). The lower level (Lower Complex) is built up by yellowish to yellow-gray tuffs, tuffaceous sandstones and breccias (chiefly of felsic to medium composition). They are intruded by numerous differentiated subvolcanic stocks and plugs of andesite, dacite, and rhyolite. Deeper-seated intrusives of granodiorite-porphyry composition and texture can be distinguished (Vergunov, 1961; Vergunov and Vlasov, 1964; Sergeev, 1976; Piskunov and Rybin, 2000). The upper level (Upper Complex) is dominated by flows of basalt and basaltic andesite with small sub-volcanic intrusive bodies and modern andesitic stratovolcanoes.

According to previous studies (Davydov et al., 1968; Vitukhin et al., 1996), the Lower Complex is late Miocene–Pliocene in age, and hence older rocks are absent or hitherto not yet clearly identified on the island. The Lower Complex is often divided into two main formations, i.e. the Rybakov and Kamuy formations (e.g., Zhelubovsky and Pryaluhina, 1964; Bevz, 1971) although Martynov et al. (2010a) used a different classification and terminology (see below). Rocks from the *Rybakov Formation* are only exposed in the most uplifted and most deeply exhumed blocks, especially at the northern part of the island (Figs. 2 and 3). Most outcrops of the Lower Complex are part of the *Kamuy Formation* that thus effectively constitute the backbone of the island. A structural contact exists between the latter two formations and the overlying Upper Complex. The younger lavas of the Upper Complex are grouped in the so-called *Fregat Formation* (Gladenkov et al., 1998).

2.2. The Lower Complex and the Rybakov and Kamuy formations

The Rybakov Formation is primarily an andesitic volcanic complex, associated with mainly fine-grained tuffs, tuffaceous silt- and sand-stones, volcaniclastic sandstones, grits, conglomerates and breccias. Very often these rocks form lenses and beds of variable thickness. Some of the deposits are interpreted as turbidites (Kovtunovitch et al., 2002). The Rybakov deposits are intruded by numerous small, co-magmatic and younger sub-volcanic and plutonic bodies. The thickness of the Formation exceeds 600 m, the base of the Formation is not exposed. Diatoms (*Denticulopsis hustedtii, Neodenticula kamtschatica*, *Thalassiosira oestrupii*) and radiolarians (*Luchnocanium nipponicum*, *Thecosphaera japonica*) found

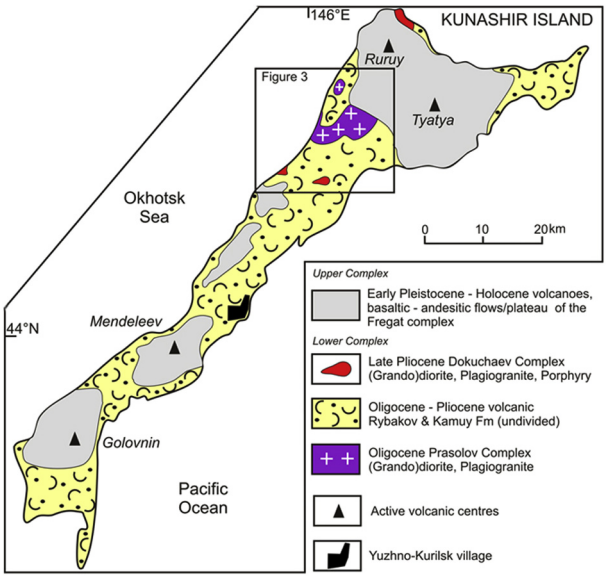

Figure 2. General geological map of Kunashir Island, southwest Kuril Islands (based on Kovtunovich et al., 2002). Location for Fig. 3 is indicated.

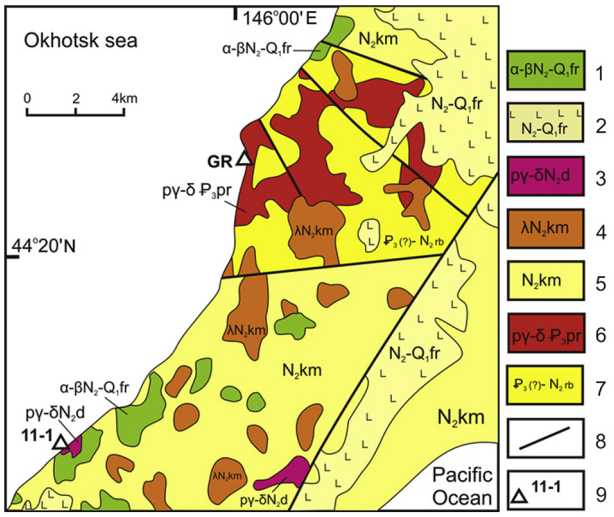

Figure 3. Detailed geological map of northern Kunashir (based on Kovtunovich et al., 2002) and indication of sample position (F-11-1 and GR) in the Dokuchaev and Prasolov sub-volcanic complexes. 1 = Late Pliocene–Pleistocene Fregat complex, andesite-basalt and basaltic sub-volcanic intrusions, stocks and dykes; 2 = late Pliocene–Pleistocene Fregat Formation, andesite-basalt and basalt flows; 3 = Pliocene Dokuchaev intrusive complex, diorite-porphyry, plagiogranite-porphyry, granodiorite-porphyry; 4 = Pliocene Kamuy Complex, dacitic stocks, necks, domes; 5 = Pliocene Kamuy Formation, dacite and rhyolite tuffs, volcanic breccia, volcanoclastic sand- and siltstones; 6 = Oligocene Prasolov intrusive complex, diorite, plagiogranite, gabbro-diorite; 7 = Oligocene(?)–early Pliocene Rybakov Formation. Andesite and dacite tuffs, volcanoclastic conglomerates, sand- and siltstones; 8 = faults; 9 = sample locations and numbers.

in the deposits, point to a late Miocene–early Pliocene age. The Rybakov Formation corresponds to what Martynov et al. (2010a) described as the Miocene Greentuff Formation and also contains the subvolcanic and deeper-seated intrusive rocks described below.

The younger Kamuy Formation principally consists of flysch-like volcanic-sedimentary deposits rich in felsic pumice of (rhyo)dacitic composition. The deposits are generally poorly or not consolidated. Rare layers of dacite and rhyolite ignimbrites and dacitic lava flows are interbedded with the main volcaniclastic flysch deposits. Lenses of conglomerates and breccias with granitic clasts as channel deposits occur in this formation. Abundant diatoms (*Thalassiosira oestrupii*, *Neodenticula kamtschatica, N. Koizumi*) and radiolarians (*Thecosphaera japonica*) constrain the Pliocene age of the Kamuy Formation (Vitukhin et al., 1996). The thickness of the Kamuy Formation exceeds 1100 m. Martynov et al. (2010a) assigned a thickness of 1500 m to what they term the Volcanic-Diatomaceous-Chert Formation.

2.3. The Upper Complex and the Fregat Formation

On Kunashir, the Rybakov and Kamuy formations (Lower Complex) are overlain by Fregat Formation (basaltic) andesitic lavas (Upper Complex, Figs. 2 and 3). A clear structural and erosional unconformity divides both complexes. The Fregat Formation contains subaerial (basaltic) andesitic lava flows, sporadically interbedded by tuffs, hyaloclastites and basaltic breccias (Syvorotkin and Rusinova, 1989). This testifies to the fact that most of the time the Fregat volcanic rocks flowed sub-aerially, while at some occasions they were deposited below sea level at shallow depths. The Fregat volcanic deposits build up a distinct volcanic plateau that formed close to sea level and was affected by posterior tectonic movements. Differential vertical movements have broken up the plateau and are responsible for the marked table-top mountainous topography of Kunashir (Syvorotkin and Rusinova, 1989). Fregat Formation can be traced to neighboring islands (Syvorotkin and Rusinova, 1989). The base of the Formation is sub-horizontal and the lower part of the Formation is delineated by basal conglomerates, grits and breccia. The upper part is represented by subaerial volcanic and pyroclastic flows and deposits of medium to mafic composition with a predominance of basaltic andesites. The thickness of the Fregat Formation is ~390 m. Differential vertical displacement of the plateau resulted in various preserved blocks. The structure within each of these is very similar and allows easy correlation with individual (basaltic) andesitic lava flows of 3–20 m thick, sometimes interbedded with pumice gravel and sandy layers of up to 5 m thick.

A late Pliocene–early Pleistocene age is assigned to the Fregat Formation based on diatoms (*Neodenticula kamtschatica - N. Koizumii*) (Kovtunovich et al., 2002) and palynology (Dunichev, 1969). This biostratigraphic age corresponds to K-Ar data from the Fregat basalts. On neighboring Iturup Island, a K-Ar age of 3.07 ± 0.05 and 1.03 ± 0.6 Ma was obtained for Fregat Mountain and Medvezhiy volcano respectively (Syvorotkin and Rusinova, 1989; Bailey, 1996; Ermakov and Shteinberg, 1999). Similar basalts on Paramushir Island were dated between 2.2 and 2.6 Ma (Syvorotkin and Rusinova, 1989). Reworked boulders from the Fregat flows are included in middle Pleistocene moraine deposits (Zhelubovsky and Pryaluhina, 1964). Paleomagnetic data obtained from the Fregat rocks indeed confirm that by far, most of the lava flows erupted during the early Matuyama (inverse) Chron (Reunion Subchron) between 2.58 and 1.95 Ma. The youngest flows exhibit normal polarity and could be from the Olduvai Subchron (1.95–1.77 Ma) (Kovtunovich et al., 2002).

Martynov et al. (2010a) used the term Basaltic Formation for the Fregat flows and Andesitic Formation for the capping active volcanoes. Flows of the Fregat Formation exhibit textural and structural indications of (mainly) terrestrial, subaerial conditions, and accumulation on a flat, low-relief surface at or close to sea-level. Currently, as mentioned, the once continuous Fregat lava plateau is broken and displaced vertically in a differential pattern and plateau remnants now occur as isolated massifs (table-top mountains and hills). The elevation difference of the Fregat base level can be used for estimating accumulated syn- and post-Pleistocene tectonic uplift. Taking eustatic fluctuations into account, this estimation shows that individual blocks of Kunashir experienced non-uniform uplift with the northern section of the island exhibiting a significant vertical displacement of over 1 km (at least 1000–1100 m), while in the south, this was only 200–300 m (Syvorotkin and Rusinova, 1989).

The late Miocene–early Pliocene Rybakov Formation was formed exclusively in subaqueous conditions. According to Dunichev (1969), the volcanic rocks of the Kamuy Formation (which he assigns to the middle Pliocene) were formed in subaerial conditions in the northern and central part of Kunashir Island, whereas in the southern part, a subaqueous environment prevailed. The middle Pliocene deposits of northern Kunashir contain several ignimbrites, attesting to sub-aerial conditions. Intensive uplift of what would become Kunashir Island started in the second half of the Pliocene (during and after the accumulation of Kamuy Formation rocks). Significant tectonic movements are inferred to have taken place between accumulation of the Kamuy and Fregat Formation in the late Pliocene, resulting in a clear unconformity between the latter. The youngest uplift postdates the early Pleistocene as it is responsible for the displacement of the Fregat lava plateau. This latest uplift stage is expressed in the northern and (north)western parts of the island where intensive uplift has resulted in differential vertical movements of the Fregat reference level exceeding 1 km. Sergeev (1976) reported that during and after a middle to late Miocene deformation event, folding of the Kunashir "basement" occurred and Miocene intrusions were emplaced. He estimated that this deformation must have been associated with at least 1.5 km of uplift and denudation. Importantly, the base of the plateau basalts of the Fregat Formation lies sub-horizontally in the southern and central parts of Kunashir, while in the northwestern (Okhotsk) block (near Prasolov Massif) the Fregat Formation is deeply eroded. At the eastern (Pacific) part of this block, the Formation has a relatively steep (up to 20°) southeastern dip. These observations show a clear Pleistocene uplift, erosion, deformation and tilting of the northern block of Kunashir. Moreover, basal layers of the Fregat Formation in the northwest are represented by conglomerates, that gradually change to volcaniclastic sandstones and siltstones to the east (Dunichev, 1969). All this points to a distinct differential uplift and denudation pattern on Kunashir, with the northwest being the most intensively affected.

2.4. Active subduction volcanoes

Four modern and active (Pleistocene–Holocene) volcanoes now characterize the landscape of Kunashir Island. These stratovolcanoes are built up by a typical alternation of lava flows and tuff deposits. The composition of these volcanic deposits is mainly basaltic-andesitic to andesitic with a minor amount of more differentiated magmas of dacitic affinity as well. This modern magmatic activity is clearly associated with subduction of the Pacific plate underneath the Okhotsk plate (Martynov et al., 2010a; Fig. 1). Tyatya volcano is one of the most active and best studied volcanoes in the Kuril arc (Nakagawa et al., 2002).

2.5. Intrusions and the Prasolov and the Dokuchaev Complexes

Both in the Lower and Upper Complexes there are numerous sub-volcanic intrusions, and in the Lower Complex even deeper-seated intrusions are found. The latter are either of co-magmatic as of more differentiated composition with respect to the host magmatic rocks. In the Rybakov Formation for example, these intrusions are stocks, dikes, and sills of basaltic, andesitic, and dacitic composition. The Kamuy Formation on the other hand mainly contains dacite stocks, necks, and dikes. Two distinct intrusive complexes represent deeper-seated magmatic rocks with no associated volcanic analogs. These are (1) the Prasolov Complex, comprising gabbro, diorite, quartz diorite, granodiorite and tonalite or plagiogranite, and (2) the Dokuchaev Complex, that includes three very small bodies of fine-grained porphyritic granodiorite and tonalite (Vergunov and Vlasov, 1964; Kovtunovich et al., 2002; Figs. 2 and 3).

The Prasolov plagiogranite (tonalite) - diorite complex in fact combines three distinct plutons: the Prasolov, Mechnikov, and Lobanov massifs (Vergunov and Vlasov, 1964; Sergeev, 1976). All these intrusive massifs are incorporated in the Rybakov Formation and covered by lava flows of the Fregat Formation. These massifs include at least two intrusive phases: a gabbro-diorite phase and a more differentiated, plagiogranite (tonalite) phase.

The Prasolov massif or pluton is the largest (18 km^2 in outcrop) and gave its name to the entire Complex. It is located on NE Kunashir (Figs. 2 and 3) and morphologically is a stock. The contacts of the Prasolov stock with the Rybakov Formation rocks are mainly tectonic, but, albeit far less frequent, intrusive contacts with contact aureoles are observed as well. These aureoles of intensely thermally metamorphosed country rock are a few tens of centimeter thick and are characterized by quartz-biotite hornfels. The intrusive contacts fade out into exocontact alteration zones propagating up to few hundred meters in the country rock.

A relative late Miocene–Pliocene age of the Prasolov Complex is inferred from the intrusive contacts with rocks of the Rybakov Formation and the presence of pebbles from the Prasolov Complex granitoids in the sediments of the Kamuy Formation. Moreover, smaller sub-volcanic intrusions and dikes of the Kamuy Formation cross-cut the rocks of the Prasolov Complex. Absolute radiometric ages for the Complex span a large interval. K-Ar ages obtained for the Prasolov stock range from 61 ± 12 to about 10 Ma (most frequent 11–10 Ma ages are found) (Rybin, 1994). K-Ar ages of the rocks from the Mechnikov massif (Prasolov Complex) range from 48 ± 4 to 6 ± 2 Ma (most frequent 15–6 Ma) (Rybin, 1994). In this paper, granodiorite from Prasolov stock (GR) was sampled for radiometric dating purposes to get a better time constraint on its formation and its subsequent cooling and exhumation.

The Dokuchaev granitoid Complex is younger. It includes three small stocks, that cross-cut the Kamuy Formation (Figs. 2 and 3). Intrusive contacts of the stocks with the Kamuy host rock are observed and Kamuy xenoliths are present (Vergunov and Vlasov, 1964). The Dokuchaev Complex, composed of tonalite-porphyry, granodiorite-porphyry and diorite-porphyry, is in fact an amalgamate of three separate intrusive massifs: Dokuchaev, Valentina and Orlov. The Valentina massif, is a tonalite-porphyry stock that crops out along a 0.7 km^2 area at the Okhotsk shore in the northern part of Kunashir (Figs. 2 and 3). From this stock a sample (F-11-1) was collected for radiometric dating. In contrast to most of the Dokuchaev Complex contacts with its host rock, the contacts of the Valentina massif are tectonic rather than intrusive. A Pliocene age for Dokuchaev is proposed based on geological and K-Ar data. The composing massifs of the Dokuchaev Complex cross-cut the Pliocene Kamuy Formation and are themselves covered by early Pleistocene Fregat flows. In the basal conglomerates of the Fregat Formation, pebbles, gravels and boulders of tonalite-porphyry, similar to rocks of the Dokuchaev Complex, are found (Rybin, 1994). K-Ar ages of rocks from the Dokuchaev Complex are reported as 6.5–4.2 Ma, i.e. latest Miocene–early Pliocene (Rybin, 1994).

3. Samples and methods

Samples were taken on the western shore of Kunashir island, towards the Okhotsk Sea (Fig. 3). Two samples from sub-volcanic magmatic suites were collected on the island. These locations constitute two distinct and rare locations were relatively coarser grained, differentiated and unaltered igneous rocks can be sampled. They therefore formed the prime targets for apatite and zircon extraction and subsequent geochronologic work. The northern sample ("GR") is a finegrained, holocrystalline tonalite – granodiorite (normalized values of 30% quartz, 60% plagioclase, 10% alkali-feldspar) from the Prasolov stock. The sample contains 10–15% hornblende and important accessory minerals include zircon, apatite, monazite and titanite. The location of sample GR was measured by GPS as 44°22′16.0″N, 146°00′35.6″E.

The second sample (F-11-1) was taken somewhat more to the south (44°15′50.5″N; 145°54′44.5″E), in the granodiorite – porphyry stocks of the Dokuchaev complex. More specifically the sample originates from the small (0.7 km^2) Valentina stock (Fig. 3). F-11-1 is a fine-grained, porphyritic tonalite – granodiorite (normalized values of 35% quartz, 55% plagioclase, 10% alkali-feldspar) containing up to 15% of hornblende and 5% of biotite. Important accessory minerals here include apatite, ilmenite and magnetite.

Zircons from sample GR were handpicked and mounted in epoxy for subsequent zircon U/Pb dating. Prior to analysis, the internal structures of the zircon crystals were imaged with CL (cathode-luminescene) using a JEOL JSM-6400 SEM (Scanning Electron Microscope) and reflected light microphotography. This imaging reveals clear oscillatory zoning for all analyzed zircon crystals, which is indicative for their magmatic origin (Hoskin, 2000; Corfu et al., 2003). No inherited cores were observed. Clear (no inclusions) spot sites for laser ablation were selected based on these images. zircon U/Pb analyses were performed at the Department of Analytical Chemistry (Atomic & Mass Spectrometry Unit) using LA-ICP-SF-MS (Laser Ablation-Inductively Coupled Plasma-Sector Field-Mass Spectrometry). A New Wave Research UP193HE ArF-excimer based laser ablation system, equipped with a teardrop-shaped, low-volume (<2.5 cm^3) ablation cell was used (Gerdes and Zeh, 2009; Glorie et al., 2010, 2011). Helium (admixed with Argon after the ablation cell) was used as a carrier gas to the Thermo Scientific Element XR Sector Field mass spectrometer. Instrumental details are to be found in Glorie et al. (2011). Data Reduction was performed using PepiAge (Dunkl et al., 2009). Laser induced elemental fractionation and instrumental drift were corrected by Glorie et al. (2011). Standard zircon GJ-1 (Jackson et al., 2004) was measured repeatedly for reference during the entire sequence. Resulting Concordia and mean ages (Fig. 4) were calculated and plotted with Isoplot 3.0 (Ludwig, 2003). The Plešovice zircon standard (Sláma et al., 2008) was also measured multiple times throughout the sequence as internal control and accuracy check.

The apatite fission-track (AFT) method is a low-temperature thermochronological technique based on the spontaneous fission decay of ^{238}U (e.g., Wagner and Van den haute, 1992; Donelick et al., 2005). Apatite separates were embedded in epoxy, polished and analyzed with the external detector (ED) method (e.g., Wagner and Van den haute, 1992, and references therein). They were irradiated with thermal neutrons to produce induced ^{235}U fission tracks.

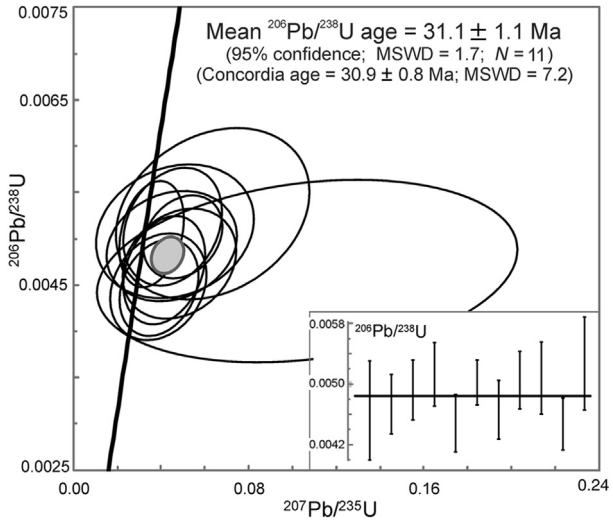

Figure 4. Concordia plot for LA-ICP-MS zircon U/Pb measurements on sample "GR" with indication of average $^{206}Pb/^{238}U$ ratio.

Spontaneous tracks in the apatite were etched with a 2.5% HNO_3 solution for 70 s at 25 °C, induced tracks in the muscovite ED with 40% HF for 40 min at 20 °C. Irradiation was performed at the Belgian Reactor 1 (BR1) facility of the Belgian Nuclear Research Centre in Mol, where the well-thermalized channel (f-ratio of 98) X26 was used (e.g., De Grave et al., 2014). AFT ages are reported as conventional ζ-ages (Hurford, 1990) with an overall weighted mean zeta of 253.1 ± 2.4 a.cm^2 (Durango and Fish Canyon Tuff apatite standards). The IRMM-540 dosimeter glass (De Corte et al., 1998) was used to monitor the thermal neutron fluence. More details on the analytical procedures can be found in other papers (e.g., Glorie et al., 2012; De Grave et al., 2013). Spontaneous and induced track densities for the Kuril samples were very low (young AFT ages and low U-concentrations), resulting in poorly constrained ages (large uncertainties; Table 2) and very low confined track densities. This latter issue also implies that no length distributions were obtained here and that hence thermal history modeling was not possible.

Apatite and zircon (U-Th)/He (AHe and ZHe respectively) analyses were performed at the John de Laeter Center for Isotope Research, Curtin University in Perth (Australia). Analytical procedures are detailed in Evans et al. (2005). Apatite grains (four replicates) from the Kunashir samples were handpicked and characterized for their morphology and dimensions and subsequently sealed in Pt micro-crucibles. Only inclusion-free grains with minimal 75 μm dimensions were selected to avoid parentless ^{4}He and to minimize Ft correction for α-ejection (Farley et al., 1996; Farley, 2002). Packages were degassed using a 1064 nm Nd-YAG laser and ^{4}He concentrations were measured by isotope dilution, after spiking with ^{3}He and calibrated against an independent ^{4}He standard, on a Pfeiffer Prisma Quadrupole mass spectrometer. Fused packages were afterwards dissolved in HNO_3, spiked with ^{235}U, ^{230}Th and ^{149}Sm and analyzed for U, Th and Sm (isotope dilution) on an Agilent Quadrupole 7500 ICP-MS. Replicate analysis of the Durango apatite age standard during this sequence yielded an average of 30.0 ± 2.5 Ma, which is in good agreement with the reported AHe age of 31.13 ± 1.01 (McDowell et al., 2005).

Zircon grains were selected and prepared in a similar fashion (using Nb instead of Pt crucibles for single grain packaging) as outlined above (also see Evans et al., 2005). Helium extraction and ^{4}He analysis was analogous as well. Dissolution of the fused zircon-Nb crucibles was done in Parr bombs at 240 °C for 40 h in a ^{235}U and ^{230}Th spiked HF solution (no Sm was measured here due to its very low concentration). After a second dissolution protocol in HCl (McInnes et al., 2009), U and Th were measured via isotope dilution as explained above for apatite.

4. Results and discussion

The Dokuchaev Complex sample (F-11-1) unfortunately did not yield a sufficient number of qualitative zircon grains to be analyzed by either U/Pb (LA-ICP-MS) or by U-Th/He. However, our second sample contained abundant suitable zircon grains. The "GR" zircons from the Prasolov Complex are typically faintly yellowish to pale orange, short bipiramidal-prismatic with a limited amount of inclusions. Prior to zircon U/Pb analysis, the embedded zircons were imaged by cathodoluminescence, which revealed a characteristic oscillatory magmatic zoning. An overview of mean parameters and zircon U/Pb results for sample "GR" of the Prasolov complex are shown in Table 1. Due to the young age of the sample and the relatively low U-concentration in the zircons, only low quantities of radiogenic Pb could be measured (~0.2–0.8 ppm). Hence, the uncertainties on the U/Pb isotopic ratios are relatively large (typically ~6–12% for the $^{206}Pb/^{238}U$ ratios and ~25–60% on the $^{207}Pb/^{235}U$ ratios). Based on the high uncertainties for the $^{207}Pb/^{235}U$ ratios and the high MSWD of 7.2 on the concordant age, the mean $^{206}Pb/^{238}U$ age of 31.1 ± 1.1 Ma is reported as the preferred zircon U/Pb age. Fig. 4 shows the plotted data on a Wetherill-Concordia curve. This 31 Ma zircon U/Pb age hence indicates that the Prasolov Complex crystallized in the early Oligocene (Rupelian). Up until now, no precise zircon U/Pb crystallization ages for this magmatic complex were known. Its age has

Table 1
Zircon LA-ICP-MS U/Pb results for sample "GR" in the Prasolov complex. For each parameter in the table, the arithmetic mean was calculated and listed. U and Pb contents (expressed as ppm) and Th/U ratio were calculated relative to the GJ-1 zircon standard. Both Pb/U and Pb/Pb ratios are corrected for: background, within-run Pb/U fractionation ($^{206}Pb/^{238}U$), where needed common Pb (Stacey and Kramers, 1975) and subsequently normalized to GJ-1 (instrumental drift corrected). 2σ values are reported in %; ρ is the error correlation defined as err($^{206}Pb/^{238}U$)/err($^{207}Pb/^{235}U$). Ages ($t_{U/Pb}$) are given as $^{206}Pb/^{238}U$ ages (calculated with Isoplot, Ludwig, 2003) in Ma with the 2σ on the age also reported in Ma.

U	Pb	Th/U	$^{206}Pb/^{238}U$	2σ	$^{207}Pb/^{235}U$	2σ	$^{207}Pb/^{206}Pb$	2σ	ρ	$t_{U/Pb}$	2σ
37	0.18	0.20	0.0047	14.0	0.1067	59.4	0.16665	57.7	0.24	29.9	4.2
73	0.33	0.23	0.0047	8.3	0.0484	35.4	0.0742	34.4	0.23	30.4	2.5
80	0.37	0.35	0.0049	8.0	0.0449	43.8	0.0662	43.1	0.18	31.6	2.5
110	0.53	0.39	0.0051	8.2	0.0453	32.9	0.0640	31.9	0.25	33.0	2.7
90	0.39	0.40	0.0045	8.5	0.0387	37.5	0.0627	36.5	0.23	28.8	2.4
166	0.80	0.45	0.0050	5.9	0.0499	23.9	0.0721	23.2	0.25	32.3	1.9
74	0.33	0.32	0.0047	8.3	0.0414	29.8	0.0645	28.6	0.28	30.0	2.5
166	0.78	0.46	0.0051	7.5	0.0356	27.3	0.0512	26.3	0.27	32.5	2.4
53	0.26	0.27	0.0051	9.4	0.0463	51.4	0.0661	50.5	0.18	32.7	3.1
14	0.45	0.37	0.0045	7.7	0.0390	30.5	0.0633	29.5	0.25	28.8	2.2
33	0.17	0.28	0.0053	11.6	0.0636	45.9	0.0875	44.4	0.25	33.9	3.9

Table 2
Top: Apatite and Zircon U-Th/He results for Kunashir island samples. For each sample 4 single grain ages were determined. Analyses in italic (GR (4), apatite) were discarded for the calculation of a sample average (see text for explanation). Ft is the alpha ejection correction parameter as defined by Farley et al. (1996). Uncorrected ages (Unc. Age) are corrected (Cor. Age) based on the Ft parameter (subdivided). TAU is the Total Analytical Uncertainty. Bottom: AFT age and length data. *n* is the number of counted grains; ρ_s, ρ_i, and ρ_d are the density of spontaneous, induced tracks and induced tracks in an external detector (ED) irradiated against a dosimeter glass; all expressed as 105 tracks/cm^2. The ρ_d-values are interpolated values from regularly spaced glass dosimeters (IRMM-540). N_s, N_i, and N_d are the number of counted spontaneous, induced tracks and induced tracks in the ED. N_d is an interpolated value. P(χ^2) is the chi-squared probability that the dated grains have a constant ρ_s/ρ_i-ratio. An ζ-value of 253.1 ± 2.4 a.cm^2 was used for the calculation of the AFT age t(ζ) (in Ma).

U-Th-Sm/He analysis

Sample	U (ppm)	1σ	Th (ppm)	1σ	Sm (ppm)	1σ	^{4}He (ncc)	err (%)	TAU (%)	Th/U	Unc. Age	1σ	Ft	Cor. Age	1σ	*Average*
Zircon																
GR (1)	759.0	15.4	519.3	10.1	–	–	0.6	2.5	3.1	0.7	1.02	0.03	0.79	1.29	0.04	
GR (2)	136.7	3.3	82.1	1.2	–	–	0.4	2.5	3.3	0.6	1.52	0.05	0.85	1.79	0.06	
GR (3)	244.9	4.7	162.5	3.2	–	–	0.1	3.8	4.2	0.7	0.81	0.03	0.77	1.05	0.04	
GR (4)	316.6	6.2	174.9	3.4	–	–	0.3	3.3	3.7	0.6	1.81	0.07	0.75	2.42	0.09	***1.64 ± 0.06***
Apatite																
GR (1)	3.68	0.16	10.87	0.45	78.5	0.9	0.001	1.3	3.1	2.9	0.49	0.02	0.75	0.65	0.04	
GR (2)	3.51	0.15	9.62	0.40	100.6	0.6	0.001	1.3	3.0	2.7	0.36	0.01	0.78	0.47	0.03	
GR (3)	3.78	0.18	9.55	0.40	85.4	0.3	0.002	0.7	3.1	2.5	1.01	0.03	0.74	1.36	0.08	***0.83 ± 0.05***
GR (4)	*4.47*	*0.19*	*8.82*	*0.37*	*64.0*	*0.5*	*0.036*	*8.3*	*8.8*	*2.0*	*12.28*	*1.08*	*0.77*	*15.99*	*1.62*	
F11 (1)	3.15	0.14	8.15	0.33	50.2	0.7	0.006	0.2	2.9	2.6	1.56	0.05	0.81	1.93	0.11	
F11 (2)	4.10	0.18	12.51	0.51	58.0	0.3	0.003	0.5	2.9	3.0	1.10	0.03	0.76	1.44	0.08	
F11 (3)	3.27	0.14	11.06	0.45	44.3	0.3	0.003	0.5	2.9	3.4	1.27	0.04	0.76	1.67	0.10	
F11 (4)	3.26	0.14	9.74	0.40	48.7	0.2	0.008	0.2	2.9	3.0	2.14	0.06	0.80	2.68	0.15	***1.93 ± 0.11***

AFT analysis

Sample	*n*	ρ_s (±1σ)	N_s	ρ_i (±1σ)	N_i	ρ_d (±1σ)	N_d	ρ_s/ρ_i	P(χ^2)	Age$_\zeta$ (Ma)
GR	11	0.043 (0.025)	3	0.455 (0.080)	32	3.229 (0.070)	2099	0.064 ± 0.038	0.95	2.6 ± 1.6
F11-1	29	0.065 (0.019)	12	0.566 (0.055)	105	3.208 (0.071)	2053	0.076 ± 0.023	0.99	3.1 ± 1.0

always been inferred from relative geological relations to host rocks where biostratigraphic ages could be obtained (e.g., based on radiolarians and diatoms), and from K-Ar dating. The latter technique however often only elucidates the timing of post-magmatic cooling in this respect and moreover is easily disturbed by posterior heating events. K-Ar ages on plutonic rocks therefore often underestimate the true emplacement ages of the intrusion. The new data presented here show that the age of the Prasolov Complex is more ancient than previously thought. Based on biostratigraphy and K-Ar dating, the Prasolov Complex has hitherto been assigned a late Miocene–Pliocene age, although an older K-Ar age of 61 ± 12 Ma (early Palaeocene) has been reported as well (Rybin, 1994). The K-Ar ages however were poorly constrained and most commonly they cluster around ~10 Ma (late Miocene).

Our more reliable zircon U/Pb age of 31 Ma now shows that the Prasolov (grano)diorite – tonalite crystallized in the early Oligocene. This obviously has its implications for the age of the host rocks of the Rybakov Formation as well. As the Prasolov rocks are clearly intruded in the tuffs, and tuffaceous–volcanogenic sediments of the Rybakov Formation, the Prasolov Complex does not constitute the basement for the Rybakov deposits. The age of the latter therefore must be similar or predate 31 Ma. This implies that deposition of the Rybakov Formation was already underway in the early Oligocene, which is significantly older that envisaged hitherto. The structure and stratigraphy of the Rybakov Formation might therefore be more complex and might incorporated more (and older) members than previously thought. All volcanic and clastic deposits of Kunashir Island were considered to be of Neogene age, our data indicates that at least some rocks of the Lower Complex are Palaeogene. This also holds true for most of the main Kuril Arc, where volcanic deposits are thought to have started accumulating in the early–middle Miocene (e.g., Martynov et al., 2010a). These authors do not exclude the possibility that development might have begun somewhat earlier in the Oligocene. The data obtained here on the Prasolov Complex on Kunashir Island now clearly show that this was indeed the case, and that these events even transpired in the Rupelian of the early Oligocene at or even before ~31 Ma.

From sample GR from the Prasolov Complex, zircons were also prepared for U-Th/He analysis (ZHe). No Sm was measured. The resulting data are listed in Table 2. In addition also apatites from sample GR were separated, as well as apatites from sample F-11-1 from the Dokuchaev Complex. The latter magmatic complex crops out somewhat more to the south on the Okhotsk Sea coast of Kunashir Island with respect to the Prasolov Complex (Fig. 3). The apatites were prepared for both apatite fission-track (AFT) as well as for apatite U-Th-Sm/He thermochronology. Table 2 includes the apatite U-Th-Sm/He (AHe) results for GR and F-11-1 and AFT results for sample GR. While the apatites for both samples generally are abundant and of moderate to good quality (euhedrical, prismatic crystals; clear with no or little inclusions), an AFT analysis was difficult to perform due to the very low spontaneous (ρ_s) and induced track densities (ρ_i) making it very hard to extract statistically viable results. These low values prove to be the consequence of both low U concentration (3–4 ppm, Table 2) and of a young AFT age. In several cases ρ_s-values are zero as several grains did not exhibit spontaneous tracks after etching and actually represent zero-age grains. The latter issues make the AFT ages statistically poorly constrained and the values should be treated with some caution. However, as they are supported by both the AHe and ZHe ages, they were added here, and in tandem with aforementioned techniques, show that the sampled rocks were subjected to rapid Plio–Pleistocene cooling (Fig. 5).

As can be deduced from the AHe and ZHe data and the AFT data in Table 2, both the sampled complexes experienced significant cooling and exhumation in the late Pliocene–Quaternary (Fig. 5). In all but one case, reproducible He-ages were obtained on four single grain aliquots. Apatite grain "4" for the Prasolov sample GR however exhibits a deviantly high age due to an anomalously high ^{4}He yield (Table 2). This is probably caused by parentless radiogenic He-gas, trapped in the apatite lattice, coming from an undetected U and/or Th rich inclusion. The result on this grain was hence omitted and not withheld in the average age calculation.

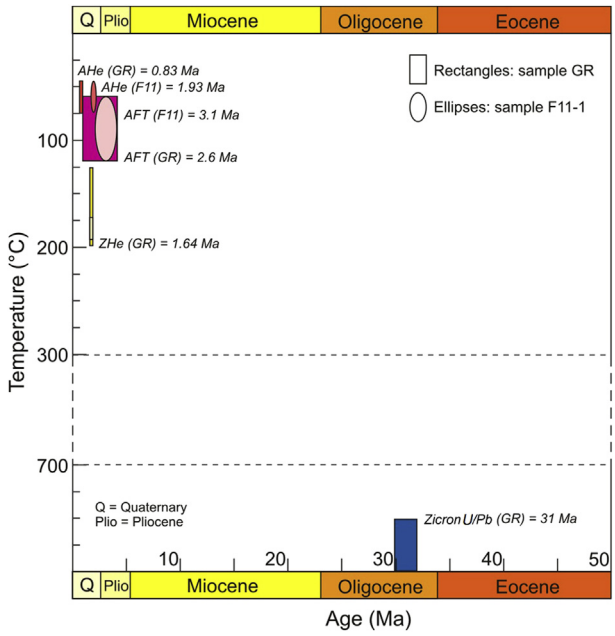

Figure 5. Overview of the ages for both samples obtained with the different dating methods in a time-temperature space. Each of the methods used (AHe = apatite U-Th-Sm/He dating; AFT = apatite fission-track dating; ZHe = zircon U-Th/He dating) is characterized by a method-specific closure temperature. See text for further explanation.

He-ages are typically cooling ages and are used in thermochronometry to document the time a certain apatite- or zircon-bearing rock passed through the closure temperature at which the specific system starts registering time (starts accumulating radiogenic daughter product). More specifically, in He-termochronometry, AHe and ZHe ages record when the analyzed apatites and zircons respectively, passed through a partial retention zone, to within a temperature window where He-gas becomes immobile and does not leak from the particular crystal lattice. They hence pinpoint when the apatite- or zircon-bearing rock cooled through the system-specific threshold. For apatite this is between about 45 and 75 °C (Fig. 5) (e.g., Ehlers and Farley, 2003), and for zircon this is approximately 150–190 °C (e.g., Reiners et al., 2004). These values strongly depend on the cooling rate, but also on the level of radiation damage (thus directly related to U and Th concentrations) a crystal has been subjected to. Recent studies (e.g., Wolfe and Stockli, 2010) have shown that because of these parameters, closure temperature windows for the ZHe system for example can vary greatly between ~130 and 200 °C (Fig. 5). AFT ages are also typically cooling ages and identifies the moment in time when the apatite-bearing rocks cooled through the ~60–120 °C temperature window (Fig. 5). This is often termed the apatite partial annealing zone (Wagner and Van den haute, 1992 and references therein). In this temperature window latent or unetched fission tracks in apatite undergo thermal track fading or shortening. At higher temperatures the apatite lattice is thermally restored and the lattice damage e.g., due to track formation (spontaneous fission decay of ^{238}U) is erased. Spontaneous or natural tracks hence are only retained when the ~60–120 °C temperature window is passed. AFT ages, based on the spontaneous track density, are therefore cooling ages beneath this threshold.

The Prasolov He-ages (Table 2), for both the zircon and the apatite systems, are Pleistocene (Calabrian Stage). In particular, the average ZHe age is calculated as 1.64 ± 0.06 Ma and the AHe age is 0.83 ± 0.05 Ma. The AFT ages are far less constrained, and, as mentioned, due to very low spontaneous track densities, have large uncertainty ranges. For the Prasolov sample this is very outspoken and yields an AFT age of 2.6 ± 1.6 Ma, roughly placing this at the Plio–Pleistocene transition. As it was shown that the emplacement age of the Prasolov Complex is early Oligocene, ~31 Ma, the He- and AFT-ages are clearly disconnected from the intrusion event and its post-magmatic cooling. It seems unlikely that episodic Pleistocene (basaltic) andesitic lava flows on the Fregat plateau would completely reset the ZHe system (with closure temperatures of up to 200 °C) for the Prasolov rocks that are embedded in the Rybakov Formation below. Therefore the ZHe-ages are interpreted in the context of cooling of the Prasolov granitoid Complex and Rybakov Formation during post-Pleistocene break-up and differential uplift and denudation of north(west)ern Kunashir Island as explained previously (section 2.3). The fact is that the age difference between the ZHe (1.64 Ma) system (with closure temperature ~170 °C up to 200 °C) and the AHe (0.83 Ma) system (with closure temperature ~60 °C) is very small (0.81 Ma), showing that the cooling and exhumation occurred very rapidly in the Pleistocene Calabrian Stage. Using these values, it can be estimated that a cooling of at least 110 °C affected the Prasolov rocks in a relatively short time span of about 0.81 Ma, or at a rate of ~135 °C/Ma. In active subduction zone magmatic arcs, geothermal gradients can easily reach 80–100 °C/km, leading to an estimate of about 1.7–1.4 km/Ma of Quaternary (Pleistocene) exhumation. It needs to be mentioned that the AHe and AFT ages are much more prone to posterior resetting during magmatic heating of the underlying complexes. Therefore it cannot be ruled out that exhumation-induced cooling is not the only factor to take into account with respect to the AHe and AFT ages obtained here. These values at least partially correspond to observations made for vertical displacement and erosion of the Pleistocene Fregat Complex in northwestern Kunashir (see section 2.3). As mentioned, the once continuous Fregat lava plateau that was deposited at or close to sea level, is now differentially uplifted to about 1 km and is at places deeply incised, revealing the deeper-seated and exhumed intrusive bodies as Prasolov Complex. These features are most outspoken in the northwest of the island, where our samples were collected. Our data (especially the ZHe ages that are least affected by potential reheating) hence suggests that an important episode of Pleistocene exhumation of the Kuril Island arc root at Kunashir Island transpired in the early Quaternary. Again, we emphasize that in absolute terms the cooling ages might be the result of both the exhumation of the deeper-seated Prasolov Complex with superimposed posterior magmatic reheating and subsequent cooling. The exhumation of the (north)western section of Kunashir Island is taking place in the overall compressive/transpressive tectonic setting and ongoing collision of the Japan and Kuril arcs since the late Miocene (~12 Ma). It is in this setting that the Lesser Kuril Islands and the Hidaka Mountains in Central Hokkaido are being exhumed since the Miocene as well (e.g., Kawakami et al., 2004). Kusunoki and Kimura (1998) further argued that the arc-arc collision resulted in the exhumation of the lower crustal Kuril Arc rocks in East Hokkaido as mentioned previously.

Although no ZHe data is available for sample F-11-1 of the Dokuchaev Complex, located somewhat more to the south on the Okhotsk coast of Kunashir Island, the AHe age (Table 2) suggests that cooling and exhumation in this block of the island (Fig. 3) was less intensive. Its AHe age was calculated as 1.93 ± 0.11 Ma. Also the less constrained AFT ages point to this, as they are also slightly older than is the case for sample GR from the Prasolov Complex. Here an AFT age of 3.1 ± 1.0 Ma is obtained (Table 2), corresponding to the late Pliocene. Due to the lack of zircons, no zircon U/Pb emplacement age for this intrusive complex could be constrained here, but relative dating suggests that the Dokuchaev Complex, embedded in the Kamuy Formation, is of early Pliocene age. K-Ar data (Rybin,

1994) indicated its emplacement should predate 4 Ma. Our AHe age of ~2 Ma therefore shows that cooling of the complex transpired shortly after emplacement and its approximate present crustal position had already been established at that time. Further cooling and exhumation of the Dokuchaev rocks to their present outcrop position was minor compared to the Prasolov Complex.

5. Conclusions

A multi-method investigation was carried out on samples from deeper-seated intrusives in the volcanic basement of Kunashir Island, southwest Kuril arc. For the first time zircon U/Pb age information constrains the early development of the Kuril Arc. While previously only relative age information and K-Ar ages (which indicate post-magmatic cooling rather that crystallization ages) were available, a more rigid absolute age frame was presented here. Zircon U/Pb crystallization ages from a fine-grained tonalite–granodiorite in the Prasolov Complex (Fig. 2) show that the plutonic stock was emplaced ~31 Ma ago (Rupelian, early Oligocene). The stock exhibits a clear intrusive relationship with the host rocks of the Rybakov Formation, which is thought to represent the oldest deposits on the island. The results presented here, indicate that the modern Kuril volcanic islands were developing significantly earlier than previous thought (early–middle Miocene).

Thermochronometry based on ZHe and AHe dating and on AFT analyses shows a distinct differential cooling pattern of the Kunashir basement and refines our insights of its recent evolution. To the best of our knowledge these are the first thermochronologic ages reported for the upper crustal root of the Kuril Arc. The northwestern block, containing the Prasolov granitoids intruded in the rocks of the Rybakov Formation, was affected by a rapid early Quaternary cooling, passing the ZHe, the AFT and subsequently the AHe closure temperature in about 800 ka. Although obviously a high geothermal gradient is present in this active magmatic arc, it implies that the Prasolov Complex was rapidly cooled and exhumed in the early Quaternary (Calabrian Stage). The Dokuchaev Complex within the Kamuy Formation, located in a tectonic block south of the Prasolov Complex block, clearly experienced less intensive, less rapid cooling in this time frame. It reached AHe retention temperatures already by ~2 Ma ago. This data fits well with observations that the overlying, late Pliocene–Pleistocene plateau lavas of the Fregat Formation are intensely uplifted, tilted and eroded in the northern–northwestern sector of Kunashir Island.

Acknowledgements

This research was supported by a start-up grant from the Faculty of Sciences, Ghent University (JDG) and the Australian Research Council (Grant No. DP150101730). SG's contribution forms TRaX record #309. The authors wish to thank G. N. Rogotnev for assistance during fieldwork and for sharing his many insights in the regional geology of the Kuril Islands, and Dr. Andrei Izmer for assistance during zircon U/Pb analyses. Anonymous reviewers and editors are thanked for their comments which attributed to the quality enhancement of this paper.

References

Apel, E.V., Bürgmann, R., Steblov, G., Vasilenko, N., King, R., Prytkov, A., 2006. Independent active microplate tectonics of northeast Asia from GPS velocities and block modeling. Geophysical Research Letters 33, L11303. http://dx.doi.org/10.1029/2006GL026077.

Avdeiko, G.P., Volynets, O.N., Antonov, A.Y., Tsvetkov, A.A., 1991. Kurile island-arc volcanism: structural and petrological aspects. Tectonophysics 199, 271–287.

Bailey, J.C., 1996. Role of subducted sediments in the genesis of Kurile-Kamchatka island arc basalts: Sr isotopic and elemental evidence. Geochemical Journal 30, 289–321.

Bailey, J.C., Frolova, T.I., Burikova, I.A., 1989. Geochemistry and petrogenesis of Kuril Island – arc basalts. Contributions to Mineralogy and Petrology 102, 265–280.

Bailey, J.C., Larsen, O., Frolova, T.I., 1987. Strontium isotope variations in lower Tertiary – Quaternary volcanic rocks from the Kurile island arc. Contributions to Mineralogy and Petrology 95, 155–165.

Baranov, B., Wong, H.K., Dozorova, K., Karp, B., Lüdmann, T., Karanaukh, V., 2002. Opening geometry of the Kurile Basin (Okhotsk Sea) as inferred from structural data. The Island Arc 11, 206–219.

Bazhenov, M.L., Burtman, V.S., 1994. Upper Cretaceous paleomagnetic data from Shikotan Island, Kuril Arc: implications for plate kinematics. Earth and Planetary Science Letters 122, 19–28.

Bevz, V.E., 1971. Stratigraphy of Cenozoic deposits of the Iturup island (Kuril islands). Geology and Mineral resources of the Sakhalin and Kuril islands. Yuzhno-Sakhalinsk 19–31 (in Russian).

Bindeman, I.N., Bailey, J.C., 1999. Trace elements in anorthite megacrysts from the Kurile Island Arc: a window to across-arc geochemical variations in magma composition. Earth and Planetary Science Letters 169, 209–226.

Cook, D.B., Fujita, K., McMullen, C.A., 1986. Present-day plate interactions in northeast Asia: North American, Eurasian, and Okhotsk plates. Journal of Geodynamics 6, 33–51.

Corfu, F., Hanchar, J.M., Hoskin, P.W.O., Kinny, P., 2003. Atlas of zircon textures. Reviews in Mineralogy and Geochemistry 53, 469–500.

Davydov, M.N., Dunichev, V.M., Taboyakov, A. Ya, 1968. Recent data on neogene sediments of southern Group of large kuril islands (Urup, iturup, kunashir). Russian Geology and Geophysics 12, 112–116.

De Corte, F., Bellemans, F., Van den haute, P., Ingelbrecht, C., Nicholl, C., 1998. A new U doped glass certified by the European Commission for the calibration of fission-track dating. In: Van den haute, P., De Corte, F. (Eds.), Advances in Fission-track Geochronology. Kluwer Academic Publishers, Dordrecht, pp. 67–78.

De Grave, J., Buslov, M.M., Van den haute, P., 2007. Distant effects of India-Eurasia convergence and Mesozoic intracontinental deformation in Central Asia: constraints from apatite fission-track thermochronology. Journal of Asian Earth Sciences 29, 188–204.

De Grave, J., Glorie, S., Buslov, M.M., Stockli, D.F., McWilliams, M.O., Batalev, V., Van den haute, P., 2013. Thermo-tectonic history of the Issyk-Kul basement (Kyrgyz Northern Tien Shan, Central Asia). Gondwana Research 23, 998–1020.

De Grave, J., De Pelsmaeker, E., Zhimulev, F.I., Glorie, S., Buslov, M.M., Van den haute, P., 2014. Meso-Cenozoic building of the northern Central Asian Orogenic Belt: thermotectonic history of the Tuva region. Tectonophysics 621, 44–59.

Donelick, R., O'Sullivan, P., Ketcham, R., 2005. Apatite fission-track analysis. Reviews in Mineralogy and Geochemistry 58, 49–94.

Dunichev, V.M., 1969. Neogene sedimentary-volcanogenic formations of Kunashir island (Kuril islands) and their relation with endogenous mineralization. Russian Geology and Geophysics 1, 131–135 (in Russian).

Dunkl, I., Mikes, T., Frei, D., Gerdes, A., von Eynatten, H., 2009. PepiAGE: data reduction program for time-resolved U/Pb analyses - Introduction and call for tests and discussion. University of Goettingen Publication, p. 15. http://www.sediment.uni-goettingen.de/staff/dunkl/zips/PepiAGE-introduction-c1.pdf.

Ehlers, T.A., Farley, K.A., 2003. Apatite (U-Th)/He thermochronometry: methods and applications to problems in tectonic and surface processes. Earth and Planetary Science Letters 206, 1–14.

Ermakov, V.A., Shteinberg, G.S., 1999. Kudryavyi Volcano and the evolution of the Medvezhiya caldera (Iturup island, Kuril islands). Journal of Volcanology and Seismology 21, 307–338.

Evans, N.J., Byrne, J.P., Keegan, J.T., Dotter, L.E., 2005. Determination of Uranium and Thorium in zircon, apatite, and Fluorite: application to laser (U-Th)/He thermochronology. Journal of Analytical Chemistry 60, 1159–1165.

Farley, K.A., 2002. (U-Th)/He dating: techniques, calibrations, and applications. In: Noble Gas geochemistry. Reviews in Mineralogy and Geochemistry 47, 819–844.

Farley, K.A., Wolf, R.A., Silver, L.T., 1996. The effects of long alpha-stopping distances on (U-Th)/He ages. Geochimica et Cosmochimica Acta 60, 4223–4229.

Fournier, M., Jolivet, L., Huchon, P., Sergeyev, K.F., Oscorbin, L.S., 1994. Neogene strike-slip faulting in Sakhalin and the Japan Sea opening. Journal of Geophysical Research 99, 2701–2725.

Gerdes, A., Zeh, A., 2009. Zircon formation versus zircon alteration - new insights from combined U-Pb and Lu-Hf in-situ LA-ICP-MS analyses, and consequences for the interpretation of Archean zircon from the Central Zone of the Limpopo Belt. Chemical Geology 261, 230–243.

Gladenkov, Yu. B., Salnikov, B.A., Borovtsev, A.V., Kovtunovich, P. Yu, 1998. Solutions by the Interdepartmental Regional Stratigraphic Workshops: Paleogene and Neogene Eastern Russia - Kamchatka, Koryak Upland, Sakhalin and Kuilskih Islands. (Explanatory Note to Stratigraphic Schemes). Moscow, p. 147 (in Russian).

Glorie, S., De Grave, J., Buslov, M.M., Elburg, M.A., Stockli, D.F., Van den haute, P., Gerdes, A., 2010. Multi-method chronometric constraints on the evolution of the Northern Kyrgyz Tien Shan batholith: from emplacement to exhumation. Journal of Asian Earth Sciences 38, 131–146.

Glorie, S., De Grave, J., Buslov, M.M., Zhimulev, F.I., Izmer, A., Vandoorne, W., Ryabinin, A., Van den haute, P., Vanhaecke, F., Elburg, M., 2011. Formation and

Palaeozoic evolution of the Gorny-Altai - Altai-Mongolia suture zone (South Siberia): zircon U/Pb constraints on its igneous record. Gondwana Research 20, 465–484.
Glorie, S., De Grave, J., Zhimulev, F.I., Buslov, M.M., Elburg, M.A., Van den haute, P., 2012. Structural control on Meso-Cenozoic tectonic reactivation and denudation in the Siberian Altai: Insights from multi-method thermochronometry. Tectonophysics 544-545, 75–92.
Hoskin, P.W.O., 2000. Patterns of chaos: fractal statistics and the oscillatory chemistry of zircon. Geochimica et Cosmochimica Acta 64, 1905–1923.
Hurford, A.J., 1990. Standardization of fission track dating calibration: recommendation by the Fission Track Working Group of the I.U.G.S. Subcommission on Geochronology. Chemical Geology (Isotope Geoscience Section) 80, 171–178.
Jackson, S.E., Pearson, N.J., Griffin, W.L., Belousova, E.A., 2004. The application of laser ablation-inductively coupled plasma-mass spectrometry to in situ U–Pb zircon geochronology. Chemical Geology 211, 47–69.
Jolivet, L., Tamaki, K., Fournier, M., 1994. Japan Sea opening history and mechanism: a synthesis. Journal of Geophysical Research 99, 22237–22259.
Kawakami, G., Arita, K., Okada, T., Itaya, T., 2004. Early exhumation of the collisional orogen and concurrent infill of foredeep basins in the Miocene Eurasian–Okhotsk Plate boundary, central Hokkaido, Japan: Inferences from K–Ar dating of granitoid clasts. The Island Arc 13, 359–369.
Kimura, G., 1981. Tectonic evolution and stress field in the southwestern margin of the Kuril Arc. Journal of the Geological Society of Japan 87, 757–768.
Kimura, G., 1986. Oblique subduction and collision: forearc tectonics of the Kuril arc. Geology 14, 404–407.
Kovtunovich, P. Yu., Safronov, A.D., Udodov, V.V., Rashepkina, E.V., Rudenko, E.A., 2002. Explanatory Notes on the *Geology Map of Russia*, Scale 1/200 000, Kuril Series, Sheets L-55-XXII, L-55-XXVIII, L-55-XXXIV, L-55-XXIII, L-55-XXIX, L-55-XXXIII, K-55-II, L-55-XXXII. VSEGEI, St-Peterburg, p. 268 (in Russian).
Kusunoki, K., Kimura, G., 1998. Collision and extrusion at the Kuril – Japan arc junction. Tectonics 17, 843–858.
Ludwig, K., 2003. User's Manual for isoplot 3.00, a geochronological Toolkit for Microsoft Excel. Berkeley Geochronology Center Special Publication 4.
Maeda, J., 1990. Opening of the Kuril Basin deduced from the magmatic history of Central Hokkaido, North Japan. Tectonophysics 174, 235–255.
Martynov, A.Yu., Kimura, J.I., Martynov, Yu.A., Rybin, A.V., 2010a. Geochemistry of late Cenozoic lavas on Kunashir Island, Kurile arc. The Island Arc 19, 86–104.
Martynov, Yu.A., Khanchuk, A.I., Kimura, J.I., Rybin, A.V., Martynov, A.Yu., 2010b. Geochemistry and petrogenesis of volcanic rocks in the Kuril Island Arc. Petrology 18, 489–513.
McDowell, F.W., McIntosh, W.C., Farley, K.A., 2005. A precise ^{40}Ar–^{39}Ar reference age for the Durango apatite (U–Th)/He and fission-track dating standard. Chemical Geology 214, 249–263.
McInnes, B.I.A., Evans, N.J., McDonald, B.J., Kinny, P.D., Jakimowicz, J., 2009. Zircon U-Th-Pb-He double dating of the Merlin kimberlite field, Northern Territory, Australia. Lithos 1125, 592–599.
Molnar, P., Tapponnier, P., 1975. Cenozoic tectonics of Asia: effects of a continental collision. Science 189, 419–426.
Nakagawa, M., Ishizuka, Y., Kudo, T., Yoshimoto, M., Hirose, W., Ishizaki, Y., Gouchi, H., Katsui, Y., Solovyow, A.W., Steinberg, G.S., Abdurakhmanov, A.I., 2002. Tyatya volcano, southwestern Kuril arc: recent eruptive activity inferred from widespread tephra. The Island Arc 11, 236–254.
Piskunov, B.N., Rybin, A.V., 2000. Petrogeochemical types of granitoids of the Kuril island arc. Doklady Earth Science 371, 93–95.
Reiners, P.W., Spell, T.L., Nicolescu, S., Zanetti, K.A., 2004. Zircon (U-Th)/He thermochronometry: He diffusion and comparisons with Ar-40/Ar-39 dating. Geochimica et Cosmochimica Acta 68, 1857–1887.
Rybin, A.V., 1994. Intrusive rocks of the Main Kuril ridge: petrography and petrogenesis. Yuzhno-Sakhalinsk 58 (in Russian) preprint, Institute of Marine Geology and Geophysics FEB RAS.
Savostin, L., Zonenshain, L., Baranov, B., 1983. Geology and plate tectonics of the Sea of Okhotsk. In: Hilde, T., Uyeda, S. (Eds.), Geodynamics of the Western Pacific – Indonesian region. AGU Geodynamics Series, 11, pp. 189–221.
Schellart, W.P., Jessell, M.W., Lister, G.S., 2003. Asymmetric deformation in the backarc region of the Kuril arc, northwest Pacific: new insights from analogue modeling. Tectonics 22 (5), 1047.
Seno, T., Sakurai, T., Stein, S., 1996. Can the okhotsk plate be discriminated from the North American plate? Journal of Geophysical Research 101 (11), 305–315.
Sergeev, K.F., 1976. Tectonics of the Kuril Island System. Nauka, Moscow, p. 240 (in Russian).
Sláma, J., Košler, J., Condon, D.J., Crowley, J.L., Gerdes, A., Hanchar, J.M., Horstwood, M.S.A., Morris, G.A., Nasdala, L., Norberg, N., Schaltegger, U., Schoene, B., Tubrett, M.N., Whitehouse, M.J., 2008. Plešovice zircon –A new natural reference material for U–Pb and Hf isotopic microanalysis. Chemical Geology 249, 1–35.
Stacey, J.S., Kramers, J.D., 1975. Approximation of terrestrial lead isotope evolution by a two-stage model. Earth and Planetary Science Letters 26, 207–221.
Syvorotkin, V.L., Rusinova, S.V., 1989. Is there a lava plateau on the Kunashir island? Pacific geology 4, 103–108.
Tararin, I.A., Lelikov, E.P., Itaya, T., 2000. Pleistocene submarine volcanism in the Eastern Kuril Basin, sea of okhotsk. Doklady Earth Sciences 371, 366–370.
Vergunov, G.P., 1961. On Intrusive Rocks of the Southern Kuril Islands (Shikotan, Kunashir, Urup) Russian Geology and Geophysics, 5, pp. 77–80 (in Russian).
Vergunov, G.P., Vlasov, G.M., 1964. Magmatism and metamorphism/Kuril islands/Intrusive rocks, pp. 567–581. In: Geology of the USSR, 31, Part 1, Kamchatka. Kuril and Komandor islands, Moscow, p. 733 (in Russian).
Vitukhin, D.I., Oreshkina, T.V., Pushcharovskii, Yu. M., Tsukanov, N.V., 1996. New data on the geology of the Iturup island (Kuril island arc). Stratigraphy and Geological Correlation 4 (6), 61–74.
Wagner, G.A., Van den haute, P., 1992. Fission Track-dating. Kluwer Academic Publishers, Dordrecht, p. 285.
Wakita, K., 2013. Geology and tectonics of Japanese Islands: a review – the key to understanding the geology of Asia. Journal of Asian Earth Sciences 72, 75–87.
Wolfe, M.R., Stockli, D.F., 2010. Zircon (U-Th)/He thermochronometry in the KTB drill hole, Germany, and its implications for bulk He diffusion kinetics in zircon. Earth and Planetary Science Letters 295, 69–82.
Worrall, D.M., Kruglyak, V., Kunst, F., Kuznetsov, V., 1996. Tertiary tectonics of the Sea of Okhotsk, Russia: far-field effects of the India-Eurasia collision. Tectonics 15, 813–826.
Zhelubovsky, Yu. S., Pryaluhina, A.F., 1964. Stratigraphy/Kuril islands, p. 527–567. In: Geology of the USSR, 31, Part 1, Kamchatka. Kuril and Komandor islands, Moscow, p. 733 (in Russian).
Zhuravlev, D.Z., Tsvetkov, A.A., Zhuravlev, A.Z., Gladkov, N.G., Chernyshev, I.V., 1987. $^{143}Nd/^{144}Nd$ and $^{87}Sr/^{86}Sr$ ratios in recent magmatic rocks of the Kurile Island Arc. Chemical Geology 66, 227–243.